frontiers | Frontiers in Earth Science

TYPE Original Research
PUBLISHED 06 January 2023
DOI 10.3389/feart.2022.1030501

OPEN ACCESS

EDITED BY
Reza Rezaee,
Curtin University, Australia

REVIEWED BY
Junjian Zhang,
Shandong University of Science and Technology, China
Yanhui Yang,
Henan University of Urban Construction, China

*CORRESPONDENCE
Hewu Liu,
hwliu65@163.com

SPECIALTY SECTION
This article was submitted to Economic Geology,
a section of the journal
Frontiers in Earth Science

RECEIVED 29 August 2022
ACCEPTED 20 September 2022
PUBLISHED 06 January 2023

CITATION
Liu H, Song Y and Du Z (2023), Molecular dynamics simulation of shear friction process in tectonically deformed coal. *Front. Earth Sci.* 10:1030501. doi: 10.3389/feart.2022.1030501

Molecular dynamics simulation of shear friction process in tectonically deformed coal

Hewu Liu[1,2]*, Yu Song[3] and Zhigang Du[4]

[1]State Key Laboratory of Mining Response and Disaster Prevention and Control in Deep Coal Mines, Anhui University of Science and Technology, Huainan, China, [2]School of Earth and Environment, Anhui University of Science and Technology, Huainan, China, [3]School of Resources and Earth Science, China University of Mining and Technology, Xuzhou, China, [4]School of Civil Engineering, Luoyang Institute of Science and Technology, Luoyang, Henan, China

Shear friction is an important deformation process in tectonically deformed coals (TDCs) and is closely related to the dynamic metamorphism of coal. In the current study, we perform a molecular dynamics (MD) simulation of the shear friction process on primary structure coal. The simulation results show that coal friction is a process of energy transformation. The mechanical energy of shear friction work can lead to temperature increases and chain motion. Chain diffusion and reorientation are the two main chain motion modes during friction. Chain diffusion behavior is regular in the initial friction stage and becomes irregular in the later friction stage. The orientation change is different for various fused aromatic chains. The orientation changes of pentacenes and naphthacenes are more significant than those of the other fused aromatic chains, indicating that fused aromatic chains with a higher aspect ratio are preferentially reorientated by shear friction. It is also demonstrated that the C-O and C-N bonds in coal are more easily disassociated by shear friction. The research results directly confirm the molecular evolution during coal friction caused by shear stress.

KEYWORDS

shear friction, tectonically deformed coal, dynamic metamorphism, molecular structure, molecular dynamics simulation

1 Introduction

Tectonically deformed coals (TDCs) formed under the action of tectonic stress have significantly altered structures, including physical, optical, and even chemical structures (Hou et al., 2012; Niu et al., 2017; Zhang et al., 2019; Pan et al., 2022; Yu et al., 2022). The structural variation of TDCs directly affects the gas occurrence state (Ju and Li, 2009; Jiang et al., 2010; Zhang et al., 2022). Therefore, the development and structural deformation characteristics of TDCs must be considered when performing coal mining and coalbed methane (CBM) exploitation (Jiang et al., 2010; Fan et al., 2017; Cheng and Pan, 2020; Fan et al., 2020; Zhang et al., 2021; Fan et al., 2022). More recently, the chemical structural evolution of TDCs has become one of the hottest topics in coal research. According to the coal mechanochemistry, tectonic stress can cause coals that are mainly composed of

organic compounds to undergo dynamic metamorphism (Hou et al., 2017). Furthermore, molecular evolution, gas generation, and the formation of ultramicropores caused by dynamic metamorphism can lead to a change in the occurrence state and content of coalbed methane, which affects coal mining safety and CBM exploitation efficiency (Hou et al., 2017; Li et al., 2020; Zhang et al., 2021).

The effects of tectonic stress on TDC molecules have been discovered by many researchers. Different changes take place in various parts of TDC molecules under the influence of tectonic stress. The side chains or bridge bonds in coal molecules are preferentially disassociated into gases such as CO_x gases and even hydrocarbons when subject to tectonic stress (Xu et al., 2014; Hou et al., 2017; Liu et al., 2018). The changes in the fused aromatic structures of TDCs caused by tectonic stress are complicated; the structures can be reorientated, condensed, deformed, and even ruptured (Cao et al., 2007; Han et al., 2017; Song et al., 2019; Song et al., 2020). The condensation of aromatic structures promotes the evolution of coal molecules (Cao et al., 2007; Song et al., 2019), while the deformation and rupture of aromatic structures lead to the generation of secondary structural defects (Han et al., 2017). In addition, noncovalent bonds, which are less stable structures in coal, can be effortlessly cleaved by tectonic stress, which significantly increases the mobility of molecular segments (Liu and Jiang, 2019).

The mechanism of tectonic stress action is the key to revealing the molecular evolution process of TDCs. Many coal geology researchers have explored the molecular evolution theory of TDCs, and their work has promoted the development of coal mechanochemistry. Two mainstream hypotheses about TDC evolution mechanism have been proposed by coal researchers. Some researchers have shown that the molecular structures of coal can be altered under the influence of thermal or strain energies that are generated and transformed from the mechanical energy created by tectonic stress (Cao et al., 2007; Xu et al., 2014). More recently, based on new mechanochemistry findings, some researchers believe that tectonic stress might even directly act on chemical bonds and lead to their rotation or cleavage (Hou et al., 2017). However, these hypotheses have not been proven and need further investigation.

When TDC researchers clarify the mechanism of tectonic stress action, shear stress is the most cited type of tectonic stress (Ju and Li, 2009; Han et al., 2016; Wang et al., 2021a; Yang et al., 2021). This is because shear friction is an important deformation process in TDCs (Li et al., 2003) and can significantly alter TDC's molecular structure (Han et al., 2017; Wang et al., 2021a; Yang et al., 2021). From the perspective of geotribology, shear friction behavior can be universally found in geological bodies under relative motion (Boneh and Reches, 2018). Coal seams sandwiched between hard rock strata are preferentially dislocated along the bedding planes under the influence of regional tectonic movements (Li et al., 2003; Ju and Li, 2009). Macroscopically, the shearing dislocation of coal seams leads to the formation of low-angle faults with large-scale friction fault planes; microscopically, shear dislocation also occurs among the shattered fragments, which also leads to the formation of friction surfaces (Frodsham and Gayer, 1999; Li, 2001; Ju et al., 2004). Our previous studies have shown that shear friction is common in TDCs, and friction surfaces are well developed in different types of TDCs (Figure 1) (Liu, 2020). Furthermore, Fourier transform infrared spectrometry (FTIR) detection results indicate that the molecular structure of coal friction films in TDCs is changed under the action of shearing dislocation (Li, 2013). It is easy to appreciate that coal friction caused by shear stress plays an important role in the dynamic metamorphism of coal (Cao et al., 2007; Ju and Li, 2009). Therefore, the molecular evolution of coal induced by shear friction is explored further in this study.

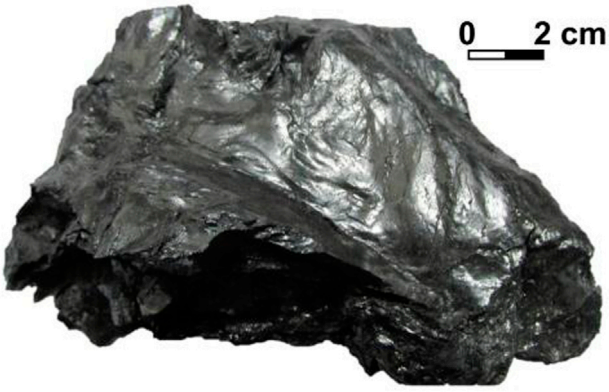

FIGURE 1
Friction surface morphologies in a TDC.

Molecular dynamics (MD) simulations have proven to be a very effective research method to reveal the molecular evolution process of coal caused by stress (Wang et al., 2021b; Yang et al., 2021). Wang et al. (2017), Wang et al. (2021a), and Wang et al. (2021b) successfully applied the MD simulation method to study the gas generation mechanism in coal under shear stress. They showed that the aromatic structure and functional groups of the molecular structure of coal could be attacked and transformed into gases (including CO_x, hydrocarbons, H_2O, and H_2) by shear stress. Yang et al. (2020) and Yang et al. (2021) used and MD simulation to investigate the influence of tensile and shear stresses on the chemical bonds in coal molecular structures. According to their simulation results, both tensile and shear stress can break the chemical bonds in coal to form free radicals. Meng et al. (2021) and Liu et al. (2022) also showed that external force could change the molecular structures of the coal matrix when they performed an MD simulation on coal nanoindentation. To the best of our knowledge, there is still a lack of studies involving the MD simulation of coal shear friction.

Therefore, an MD simulation of coal shear friction was performed in this study. A sandwich friction system was

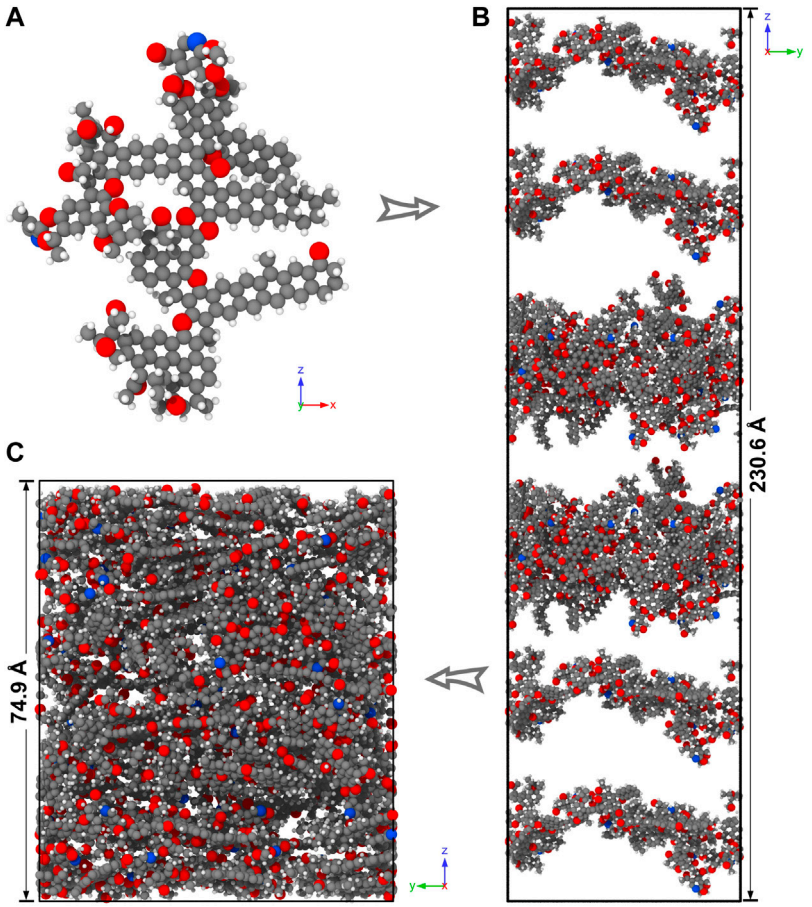

FIGURE 2
Construction procedure of the sandwich system for the shear friction simulation. (The gray refers to carbon atoms, the red refers to oxygen atoms, the blue refers to nitrogen atoms, and the white refers to hydrogen atoms.) **(A)** Conformation of the primary structure coal, **(B)** initial sandwich coal friction system, and **(C)** optimized coal friction system.

constructed and optimized based on the molecular conformation of primary structure coal. The shear friction process in a TDC was simulated by applying a constant velocity to the slider along the positive Y-axis. By clarifying the variation of temperature, energies, mean square displacement, friction force, and configuration during the friction process, the evolution of the coal's molecular structures is revealed in detail.

2 Experiment and simulation methodology

2.1 Model construction and optimization

To avoid the interference of tectonic stress in geological time, a primary structure coal from our previous research was chosen for analysis. The primary structure coal is a low-medium bituminous coal with a carbon content of 80.61% (Liu et al., 2019). Material Studio software was used to construct the conformation of the primary structure coal according to the composition and structure information obtained from elemental analysis and spectral detection results (Figure 2A). The comparison between experimental ^{13}C nuclear magnetic resonance (^{13}C NMR) spectra and simulated spectra demonstrates that the constructed conformation is very close to real coal molecules (Liu et al., 2019). The chemical formula of the built conformation is $C_{206}H_{166}N_2O_{26}$.

The sandwich coal friction system comprises two types of layers, including four thin layers and two thick layers. The thin layer consists of four conformations with a chemical formula of $C_{824}H_{664}N_8O_{104}$, and the thick layer consists of ten conformations with a chemical formula of $C_{2060}H_{1660}N_{20}O_{260}$. First, the two types of layers were constructed using the Amorphous Cell (AC) module in Material Studio. The density of the layers was set to 0.8 g/cm^3, and the

COMPASS forcefield was chosen when performing the AC calculation. Then, the atom-based summation method was used to calculate the electrostatic and van der Waals interactions between particles. Second, the initially constructed layers were optimized using the Forcite module. The geometrical structure of the layers was refined utilizing a smart method in the geometry optimization task. After the geometrical optimization, the layer structures were periodically heated and cooled in the Anneal task, and the initial and mid-cycle temperatures during the Anneal process were 298.0 K and 500.0 K, respectively. Third, the optimized layers were inserted into a simulation box to form the initial sandwich friction system ($C_{7416}H_{5976}N_{72}O_{936}$) using the Build Layers command (Figure 2B).

The initially constructed sandwich friction system did not meet all the requirements of friction simulation. Therefore, the initial system was exported from Material Studio and imported into the large-scale atomic/molecular massively parallel simulator (LAMMPS) (Plimpton, 1995) to perform the next optimization steps. First, each layer in the friction system was compressed by moving the reflecting walls along the negative Y-axis to the specified positions, and the final density of each of the layers was set to 1.0 g/cm^3, which is equal to our previous research results (Liu et al., 2019). The compression procedure was accomplished in a canonical ensemble (nvt), and the temperature of the entire system was controlled at 298.0 K through Nosé–Hoover thermostatting. Furthermore, to maintain the flat layered structure, each layer was compressed separately using the reflecting walls. The compressing procedure of each layer lasted for 2000 fs. After the layers were compressed, the redundant vacuum space above the uppermost layer was eliminated by directly changing the box size.

The compressed friction system required additional optimization to acquire a more reasonable structure. The optimization procedure follows. First, the system was heated from 298.0 K to 500.0 K with a heating rate of 0.101 K/fs in an nvt ensemble. Second, the temperature of the friction system was maintained at 500.0 K in the nvt ensemble using a Nosé–Hoover thermostat. The constant temperature heating process lasted for 200,000 fs Third, the temperature was reduced to 298.0 K, again in an isothermal-isobaric (npt) ensemble. To release the internal pressure of the friction system, 1 atm pressure was applied to the X and Y dimensions, and the "couple" keyword was used to allow the box to change in both the X and Y dimensions. The thermostatting and barostatting during the cooling process were achieved using the Nosé–Hoover method. The temperature and pressure change processes continued for 200,000 fs. Finally, the sandwich friction system was relaxed for 1,100,000 fs in an nvt ensemble, and the relaxation temperature was maintained at 298.0 K. Then, the fully optimized sandwich friction system was ready for the following shear friction simulation (Figure 2C).

2.2 Implementation of shear friction

2.2.1 Initial settings

The ReaxFF potential developed by van Duin et al. (2001) was selected to describe the pair interactions of particles, and the parameters of the C, O, N, and H particles have been previously proposed by Mattsson et al. (2010). A periodic boundary condition was applied to the X and Y dimensions, and a non-periodic and fixed boundary condition was applied to the Z dimension. The ReaxFF, which is based on the bond-order concept, is accurate enough to describe a coal's molecular evolution caused by stress (van Duin et al., 2001; Wang et al., 2021a). The six layers in the sandwich friction system play different roles during the shear friction simulation (Figure 3A). The top and bottom layers in grey were set as independent rigid bodies. The temperature of the thermal-quenched layers in blue was maintained by thermostatting at 298.0 K utilizing the Nosé–Hoover method in an nvt ensemble, which allows for the diffusion of thermal energy caused by friction. Meanwhile, the slider and free layer in purple and yellow were both set into a microcanonical (nve) ensemble, which is beneficial for the free motion of particles in these two layers during the friction process.

2.2.2 Shear friction simulation

The coal shear friction simulation can be divided into two stages. First, along the negative Z-axis, a constant normal force (0.625 MPa) was applied to each particle in the uppermost rigid layer before friction. The resultant force of the forces applied on all the particles in the rigid layer is equal to 2 GPa (number of particles (1,600) × 0.625 MPa), which significantly compresses the friction system (Figure 3B). Because of the area contact difference between nano and macro scales, the normal force in MD simulation can be several orders of magnitude larger than the actual situation (Qiang et al., 2020). The compression process continued for 400 ps to obtain a more stable friction system with almost constant total energy (Figure 4). Second, the slider was linearly moved along the positive Y-axis with a velocity of 0.005 Å/fs (500 m/s) (Figure 3B), and the shear friction of the slider lasted for 1,000 ps. The selected friction velocity in the MD simulation is much higher than the geological conditions, which can significantly accelerate the mechanolysis reaction processes of shear friction.

3 Results and discussion

3.1 The friction mode of coal

According to previous research, the interfacial contact mode of a friction system is important to determine the

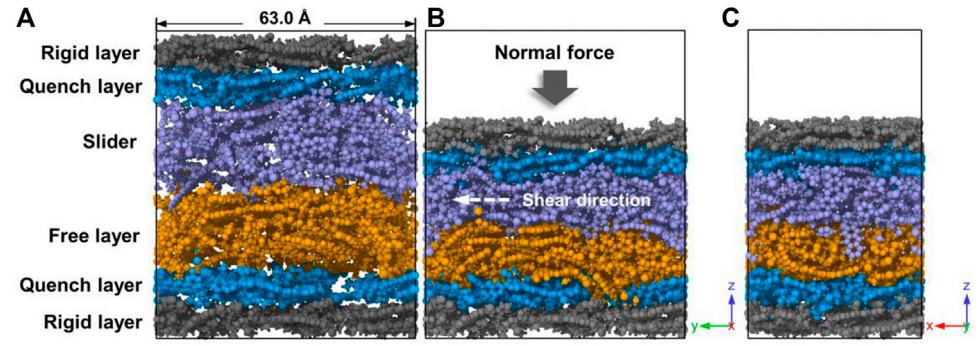

FIGURE 3
The sandwich structures of the friction system and the configuration of the friction system after compression. **(A)** The sandwich structure of the coal friction system, **(B)** the left view of the friction system after compression, and **(C)** the back view of the friction system after compression.

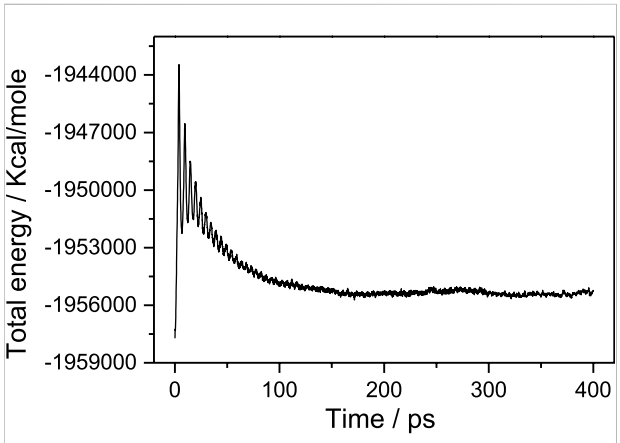

FIGURE 4
Variation of the total energy of the friction system during the compression stage.

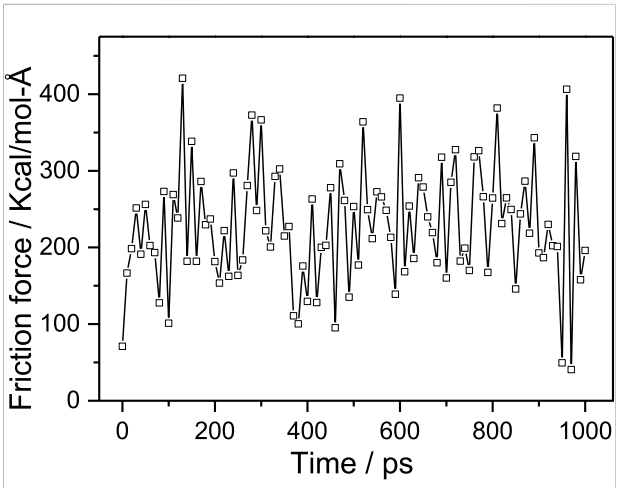

FIGURE 5
Variation of the friction force between the slider and the free layer with simulation time.

friction mode. The configuration of the friction system shows that the chains at the slider and free layer surfaces are intertwined, indicating that the interface between them is rough and robustly locked (Figures 3B,C). Generally, a rougher interface is more likely to generate a stick-slip friction mode because of the interactions of the chains at the interface (Dai et al., 2011). In this study, the friction force between the slider and the free layer steadily fluctuated between 40.5 and 420.7 Kcal/mol-Å without any regular variation (Figure 5). Therefore, the coal friction mode in the current simulation belongs to the dynamic friction type (Dai et al., 2011). The main reason for this is that the sliding velocity of 500 m/s is higher than the maximum velocity of the surface atoms in a free layer, which means that the chains in these two layer surfaces cannot adhere to each other during friction.

3.2 The frictional heating of coal

Before the friction simulation, the temperature of the entire system was maintained at 298.0 K. The temperature significantly rose to the maximum value (844.4 K) at the initial stage of friction and then decreased slightly (around 700 K) to form a plateau (Figure 6A). Studies on natural fault planes and friction experiments indicate that frictional heat can be generated during the friction between coal and other types of rocks (Bustin, 1983; Kitamura et al., 2012). Furthermore, the temperature increase caused by friction can even reach several hundred degrees (Bustin, 1983; Kitamura et al., 2012). Thus, the temperature increase in the molecular simulation is in line with actual situations.

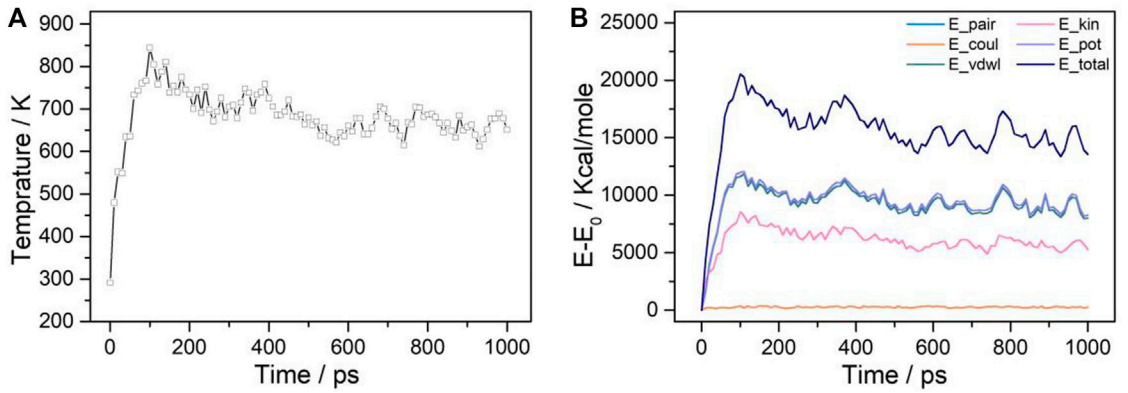

FIGURE 6
Temperature **(A)** and energy variation **(B)** of the slider during the friction process.

The shear friction work is an energy transformation process; the increasing temperature in the simulation indicates that the mechanical energy caused by shear stress is transformed into thermal energy (Hu et al., 2013). The temperature increase in the initial friction stage indicates the accumulation of thermal energy, which is closely related to the adhesive forces between interfacial atoms (Qiang et al., 2020). To start the friction process, the adhesive force between the interfacial atoms must first be overcome, which can lead to instantaneous heat generation (Qiang et al., 2020). The plateau of the temperature–time curve illustrates that less mechanical energy is dissipated in the later friction process (Rittel, 2000).

During friction, most of the mechanical energy is released through the motion of atoms and heat generation (Qiang et al., 2020). The energy difference between the energy at 0 ps(E_0) and the energy at different friction times (E) was applied to characterize the energy variation. The variation of the total energy (E_total) is basically the same as the variation in the temperature, indicating the transformation of energy into temperature (Figure 6). The total energy is the sum of other energies; therefore, the variation of the total energy is ascribed to the variation of other energies. It can be illustrated that the variation of the other types of energies also demonstrates the energy transformation process.

3.3 Chain motion during the friction process

3.3.1 Chain diffusion

Under the action of shear friction, chain motion, including chain diffusion and chain reorientation, will occur in the free layer, which can change the configuration of molecules. Mean square displacement (MSD) is commonly used to characterize chain diffusion mobility (Harmandaris et al., 1998). The slope of the MSD-time curve is positively correlated with chain diffusion mobility (Qiang et al., 2020). During the coal friction process, the MSD of the free layer increases slowly within 200 ps and then increases more significantly in the later friction stage (Figure 7).

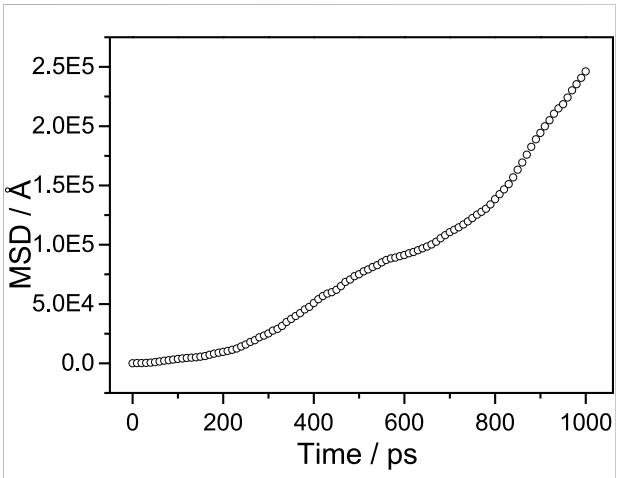

FIGURE 7
MSD variation of the slider during the friction process.

Atom trajectory analysis was performed to further reveal the chain diffusion behavior during the coal friction process. A 6 Å-thick atomic slice along the Z-axis was marked in green to analyze the chain diffusion in the free and quenched layers. Figures 8A–C depict that the shear track within 30 ps is very regular, and the track becomes very irregular after 30 ps (Figure 8D), indicating that the chain diffusion mobility increases significantly after 30 ps.

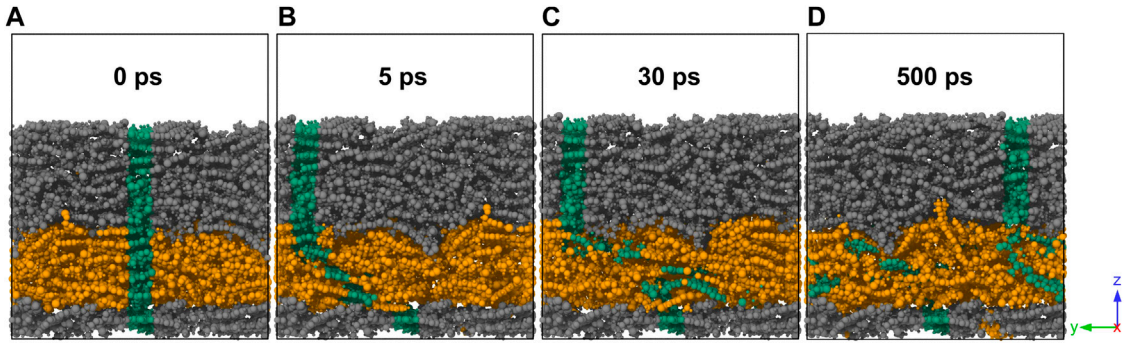

FIGURE 8
Configuration change at different shear friction times.

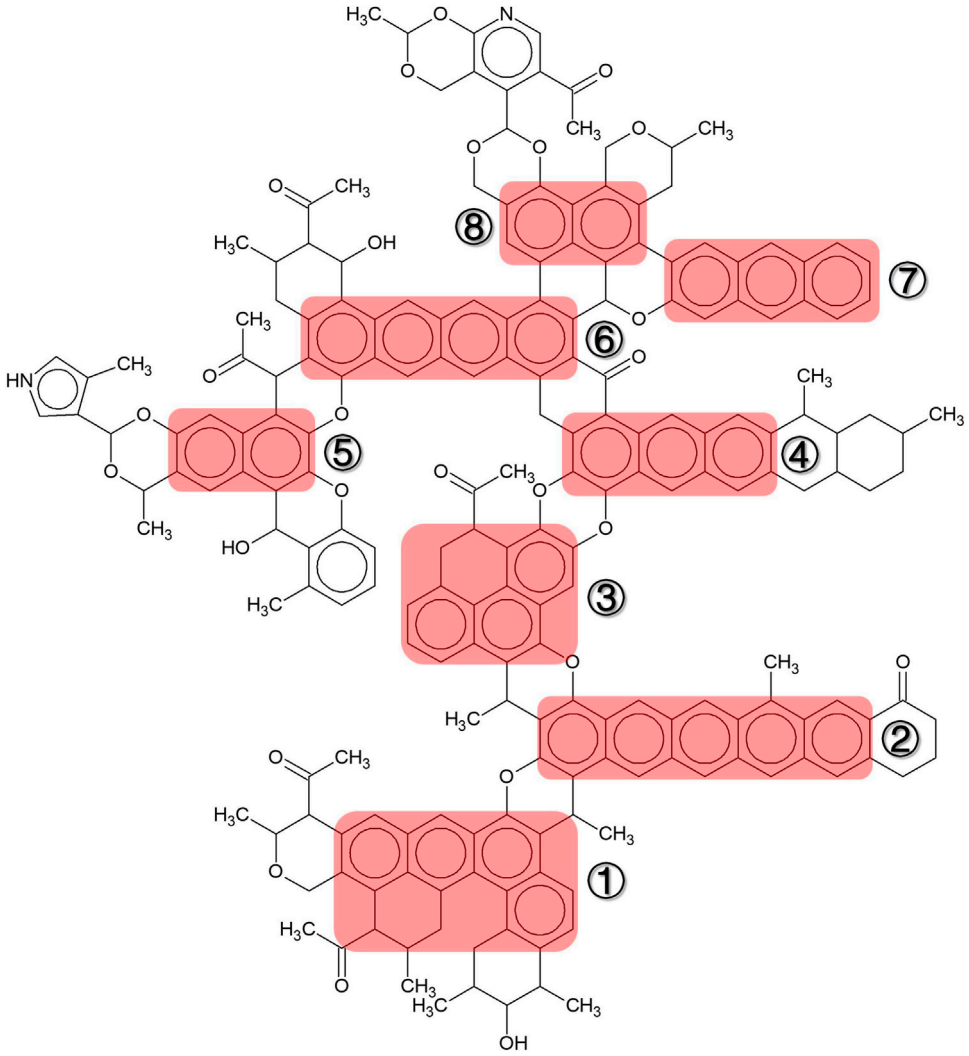

FIGURE 9
Selected fused aromatic chains in the plane model of the primary structure coal conformation. 1—Benz(a)anthracene; 2—pentacene; 3—phenanthrene; 4—anthracene A; 5—naphthalene A; 6—naphthacene; 7—anthracene B; 8—naphthalene B.

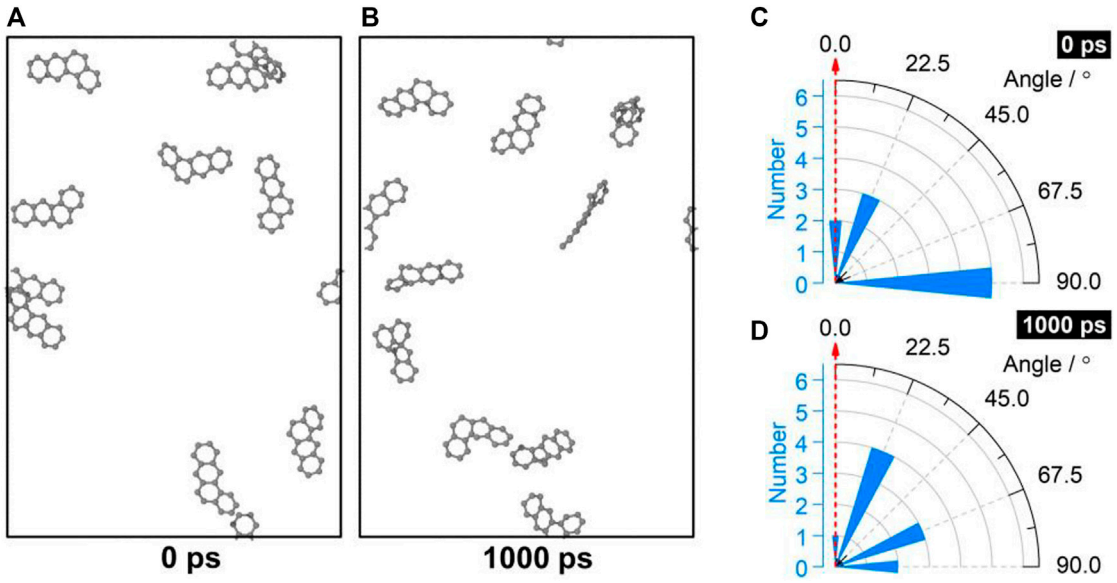

FIGURE 10
Orientation distribution of benz(a)anthracene. **(A)** and **(B)** The distribution of benz(a)anthracene at 0 ps, **(C)** and **(D)** rose diagram of the orientation of the benz(a)anthracene at 0 ps and 1,000 ps.

3.3.2 Chain reorientation

To reveal the orientation change in the friction process, the orientation of eight types of fused aromatic chains in the free layer were counted at 0 ps and 1,000 ps, respectively (Figure 9). The acute angle between the strike of fused aromatic chains (the connection between the proximal and distal C atoms) and the shear direction (the positive direction of the Y-axis) is defined as the orientation of the fused aromatic chains. The free layer is composed of ten conformations; therefore, ten acute angles can be counted for each frame (Figures 10A,B). Then, a rose diagram (0–90°) of the orientation of the fused aromatic chains can be drawn according to the statistical data (Figures 10C,D).

Among the eight types of fused aromatic chains, the benzene rings of the benz(a)anthracenes and the phenanthrenes are not in a linear arrangement, while the other six types of aromatic structures are linearly arranged. By comparing the orientation of the benz(a)anthracenes at 0 ps and 1000 ps, it can be found that five benz(a)anthracenes are in the range of 78.75–90° at 0 ps, while the number decreases to two at 1,000 ps, and more benz(a) anthracenes are rotated into the 11.25–33.75° range (Figures 10C,D). For the phenanthrenes, the orientation is mainly concentrated at 33.75–56.25°, and the number of phenanthrenes in the range of 0–33.75° increases from one to three under the action of shear friction (Figures 11C,D). Therefore, the orientation of the nonlinearly arranged aromatic chains is more parallel to the shear direction, especially for the benz(a)anthracenes.

The linearly arranged pentacenes are of the maximum length in all the aromatic chains. The orientation of the pentacenes is mainly in the range of 56.25–78.75° at 0 ps, while at 1,000 ps, the dominant orientation is within 11.25–33.75° (Figures 11A,B). The orientation angles of seven pentacenes are larger than 56.25° at 0 ps, and only two angles are in this range at 1,000 ps. Similarly, the orientations of the naphthacenes that are linear arrangements of four benzene rings are also significantly altered by shear friction. Before friction, the orientation angles of the naphthacenes mainly fall in the range of 56.25–90°, and eight angles fall into this range (Figure 11I). At the end of friction, six naphthacenes are turned parallel to the shear direction, and the orientation angles of those naphthacenes are all within the range of 0–33.75° at 1,000 ps (Figure 11J). It can be easily seen that the orientation distribution modes of the pentacenes and naphthacenes are significantly altered before and after shear fiction.

Anthracenes A and B are composed of three linearly arranged benzene rings. For anthracene A, only one orientation angle is lower than 33.75° at 0 ps, while the number increases to three at 1,000 ps by shear modification (Figures 11E,F). The orientation change of anthracene B is similar to anthracene A. Compared with the orientations at 0 ps, two more anthracene orientation angles are rotated and fall into the range of 0–33.75° at 1,000 ps (Figures 11K,L). Apart from the above change, the orientation distribution modes of anthracenes A and B remain similar at 0 ps and 1,000 ps.

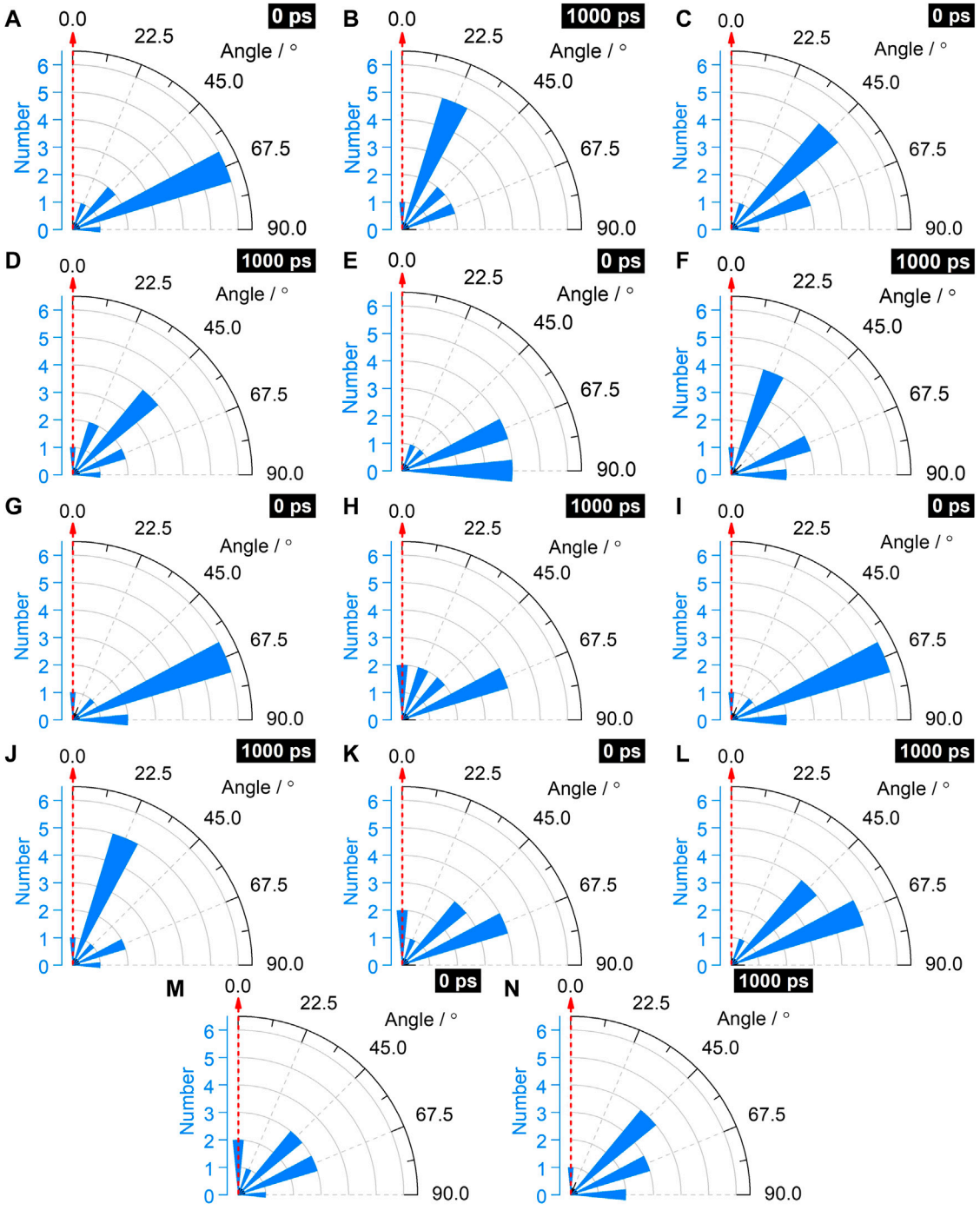

FIGURE 11
Rose diagram of the orientation of the fused aromatic chains. **(A)** and **(B)** Pentacene, **(C)** and **(D)** phenanthrene, **(E)** and **(F)** anthracene A, **(G)** and **(H)** naphthalene A, **(I)** and **(J)** naphthacene, **(K)** and (L) anthracene B, **(M)** and **(N)** naphthalene B.

Naphthalenes A and B, which are composed of two benzene rings, are the shortest among the fused aromatic chains. At 0 ps, the orientation angles of naphthalene A are mainly in the range of 56.25–90°. However, at 1,000 ps, the number of naphthalenes A with orientation angle in the range of 56.25–90° is reduced by four, and the number of naphthalenes A with orientation angle in the range of 0–33.75 is increased by four (Figures 11G,H). Compared to naphthalene A, the orientation of naphthalene B

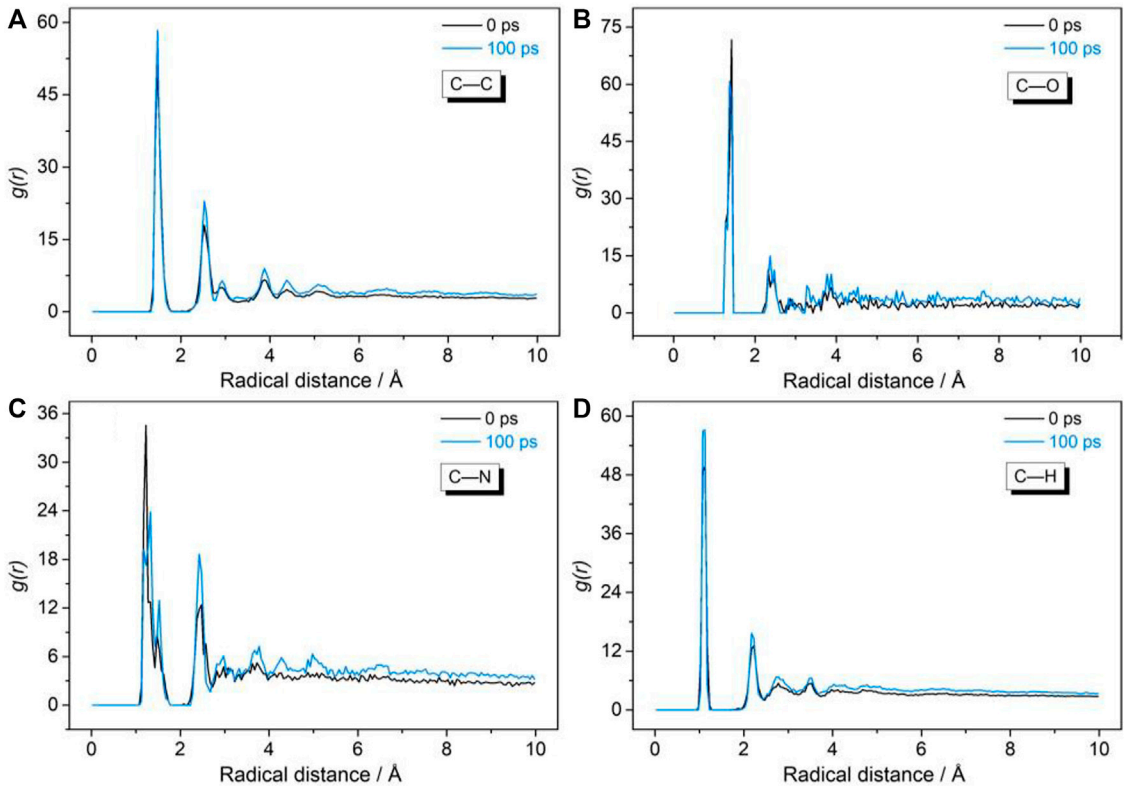

FIGURE 12
The **(A)** C-C, **(B)** C-O, **(C)** C-N, and **(D)** C-H radical distribution functions of the friction system before and after shear friction.

is less affected by shear friction. The number of orientation angles of naphthalene B within 0–33.75 is reduced from three to only one (Figure 11M,N).

In summary, under the action of shear friction, the orientation of eight types of fused aromatic chains is changed to a greater or lesser extent. The orientation change is consistent with the detection results of natural TDCs using a high-resolution transmission electron microscope (HRTEM). Order degree of the aromatic fringe of schistose and scaly coals (two types of TDCs formed in shear stress environments) observed by HRTEM is higher than that of unaltered coals, which indicates that shear stress can promote the order degree of aromatic structures (Song et al., 2020). The MD simulation results also demonstrate the orientation change behavior caused by shear friction. Furthermore, under the same shear friction conditions, the orientation change degree is different for various types of fused aromatic chains. The orientation of linearly arranged pentacenes and naphthacenes is more parallel to the shear direction at 1,000 ps than is the orientation of other types of fused aromatic chains. This is mainly because the orientation change of the fused aromatic chains is closely correlated with the aspect ratio of fused aromatic chains. Fused aromatic chains with larger aspect ratios are more prone to be reoriented by shear friction.

3.4 Atomic separation characteristics

The radial distribution function (RDF) *g(r)* is usually applied to reveal the interatomic separations and structure of molecular systems (Hua et al., 2020). The *g(r)* before and after friction is calculated to investigate the atomic interaction variation, including the interactions of C-C, C-O, C-N, and C-H atoms. The first peaks all appear within the radical distance range of 1.0–2.0 Å, which reflects the basic structural characteristic of coal molecules well (Figure 12). This is because the average nearest-neighbor distances of C-C (1.54 Å), C-O (1.43 Å), C-N (1.32 Å), and C-H (1.09 Å) are all in this range.

The intensity of the first *g(r)* peak of C-O decreases after shear friction, which may indicate that the C-O bonds have a high likelihood of being disassociated or deviated from the equilibrium position by shear stress (Hong et al., 2011) (Figure 12B). The first *g(r)* peak of C-N shifts to a higher radical distance after shear friction, which means that the neighbor distance between the carbon and nitrogen atoms becomes larger (Figure 12C). Thus, the C-N bonds of coal are also more prone to be cleaved by shear stress. In contrast, the intensities of the first peak of C-C and C-H at 1,000 ps are higher than that at 0 ps(Figures 12C,D), which may be caused by the increasing density under the action of normal force. Normal force

constantly compresses the friction system and decreases the free volume, which makes the carbon and hydrogen atoms become closer. Therefore, it can be concluded that C-O and C-N bonds are more easily disassociated by shear friction. The simulation results are consistent with the experimental results that the functional groups with heteroatoms are preferentially cleaved by tectonic stress into gases (Xu et al., 2014).

4 Conclusion

In this study, a sandwich friction system is constructed utilizing the conformation of primary structure coal. A normal force and constant shear velocity are applied to the molecular friction system to simulate the shear friction behavior. The MD simulation results are consistent with the experimental results of natural TDCs in other studies. First, coal friction is actually an energy transformation process. The shear friction work can both transform into thermal energy and lead to an increase in temperature and can also transform into kinetic energy, leading to atomic motion. Chain diffusion and reorientation are two important atomic motion types during coal friction. Atom trajectory analysis demonstrates that chain diffusion is regular within 30 ps friction, following which the diffusion behavior becomes irregular. The orientation before and after shear friction is revealed for eight types of fused aromatic chains. The fused aromatic chains are more or less reorientated by the shear friction. However, compared with the other fused aromatic chains, the orientation of pentacenes and naphthacenes are more parallel to the shear direction, indicating that the higher aspect ratio is beneficial to the reorientation caused by shear friction. Furthermore, the decreasing intensity of the first C-O peak and the radical distance shift of the first C-N peaks both indicate that the C-O and C-N bonds are preferentially cleaved by shear friction.

Data availability statement

The raw data supporting the conclusion of this article will be made available by the authors without undue reservation.

Author contributions

HL undertook the experiments, prepared the manuscript and analyzed the data; YS and ZD commented on the manuscript.

Funding

This work was supported by the National Natural Science Foundation of China (grant number 42102221), the Anhui Provincial Natural Science Foundation (grant number 2108085QD167), the Natural Science Foundation of Henan Province (grant number 222300420242), the Independent Research Fund of the State Key Laboratory of Mining Response and Disaster Prevention and Control in Deep Coal Mines (grant number SKLMRDPC20ZZ10), the Natural Science Foundation of Henan Province (grant number 222300420242), the Science and Technology Development Project of Luoyang (grant number 2101025A), the Heluo Young Talent Lifting Project of the Society and Technology Association of Luoyang (grant number 2022HLTJ06), and the Scientific Research Starting Foundation for the Introduced Talents of Anhui University of Science and Technology.

Conflict of interest

The authors declare that the research was conducted in the absence of any commercial or financial relationships that could be construed as a potential conflict of interest.

Publisher's note

References

Boneh, Y., and Reches, Z. E. (2018). Geotribology - friction, wear, and lubrication of faults. *Tectonophysics* 733, 171–181. doi:10.1016/j.tecto.2017.11.022

Bustin, R. M. (1983). Heating during thrust faulting in the rocky mountains: Friction or fiction? *Tectonophysics* 95 (3), 309–328. doi:10.1016/0040-1951(83)90075-6

Cao, D., Li, X., and Zhang, S. (2007). Influence of tectonic stress on coalification: Stress degradation mechanism and stress polycondensation mechanism. *Sci. China Ser. D.* 50 (1), 43–54. doi:10.1007/s11430-007-2023-3

Cheng, Y., and Pan, Z. (2020). Reservoir properties of Chinese tectonic coal: A review. *Fuel* 260, 116350. doi:10.1016/j.fuel.2019.116350

Dai, L., Minn, M., Satyanarayana, N., Sinha, S. K., and Tan, V. B. C. (2011). Identifying the mechanisms of polymer friction through molecular dynamics simulation. *Langmuir* 27 (24), 14861–14867. doi:10.1021/la202763r

Fan, C., Li, S., Elsworth, D., Han, J., and Yang, Z. (2020). Experimental investigation on dynamic strength and energy dissipation characteristics of gas outburst-prone coal. *Energy Sci. Eng.* 8 (4), 1015–1028. doi:10.1002/ese3.565

Fan, C., Li, S., Luo, M., Du, W., and Yang, Z. (2017). Coal and gas outburst dynamic system. *Int. J. Min. Sci. Technol.* 27 (1), 49–55. doi:10.1016/j.ijmst.2016.11.003

Fan, C., Wen, H., Li, S., Bai, G., and Zhou, L. (2022). Coal seam gas extraction by integrated drillings and punchings from the floor roadway considering hydraulic-mechanical coupling effect. *Geofluids* 2022, 1–10. doi:10.1155/2022/5198227

Frodsham, K., and Gayer, R. A. (1999). The impact of tectonic deformation upon coal seams in the South Wales coalfield, UK. *Int. J. Coal Geol.* 38 (3), 297–332. doi:10.1016/S0166-5162(98)00028-7

Han, Y., Wang, J., Dong, Y., Hou, Q., and Pan, J. (2017). The role of structure defects in the deformation of anthracite and their influence on the macromolecular structure. *Fuel* 206, 1–9. doi:10.1016/j.fuel.2017.05.085

Han, Y., Xu, R., Hou, Q., Wang, J., and Pan, J. (2016). Deformation mechanisms and macromolecular structure response of anthracite under different stress. *Energy fuels*. 30 (2), 975–983. doi:10.1021/acs.energyfuels.5b02837

Harmandaris, V. A., Mavrantzas, V. G., and Theodorou, D. N. (1998). Atomistic molecular dynamics simulation of polydisperse linear polyethylene melts. *Macromolecules* 31 (22), 7934–7943. doi:10.1021/ma980698p

Hong, Z., Hwang, S., and Fang, T. (2011). The deposition of Fe or Co clusters on Cu substrate by molecular dynamic simulation. *Surf. Sci.* 605 (1-2), 46–53. doi:10.1016/j.susc.2010.09.020

Hou, Q., Han, Y., Wang, J., Dong, Y., and Pan, J. (2017). The impacts of stress on the chemical structure of coals: A mini-review based on the recent development of mechanochemistry. *Sci. Bull.* 62 (13), 965–970. doi:10.1016/j.scib.2017.06.004

Hou, Q., Li, H., Fan, J., Ju, Y., Wang, T., Li, X., et al. (2012). Structure and coalbed methane occurrence in tectonically deformed coals. *Sci. China Earth Sci.* 55 (11), 1755–1763. doi:10.1007/s11430-012-4493-1

Hu, Y., Ma, T., and Wang, H. (2013). Energy dissipation in atomic-scale friction. *Friction* 1 (1), 24–40. doi:10.1007/s40544-013-0002-6

Hua, D., Ye, W., Jia, Q., Zhou, Q., Xia, Q., and Shi, J. (2020). Molecular dynamics simulation of nanoindentation on amorphous/amorphous nanolaminates. *Appl. Surf. Sci.* 511, 145545. doi:10.1016/j.apsusc.2020.145545

Jiang, B., Qu, Z., Wang, G. G. X., and Li, M. (2010). Effects of structural deformation on formation of coalbed methane reservoirs in Huaibei coalfield, China. *Int. J. Coal Geol.* 82 (3-4), 175–183. doi:10.1016/j.coal.2009.12.011

Ju, Y., and Li, X. (2009). New research progress on the ultrastructure of tectonically deformed coals. *Prog. Nat. Sci.* 19 (11), 1455–1466. doi:10.1016/j.pnsc.2009.03.013

Ju, Y. W., Wang, G. L., Jiang, B., and Hou, Q. L. (2004). Microcosmic analysis of ductile shearing zones of coal seams of brittle deformation domain in superficial lithosphere. *Sci. China Ser. D.* 47 (5), 393–404. doi:10.1360/02yd0291

Kitamura, M., Mukoyoshi, H., Fulton, P. M., and Hirose, T. (2012). Coal maturation by frictional heat during rapid fault slip. *Geophys. Res. Lett.* 39 (16), a–n. doi:10.1029/2012GL052316

Li, H., Ogawa, Y., and Shimada, S. (2003). Mechanism of methane flow through sheared coals and its role on methane recovery☆. *Fuel* 82 (10), 1271–1279. doi:10.1016/S0016-2361(03)00020-6

Li, H. Y. (2001). Major and minor structural features of a bedding shear zone along a coal seam and related gas outburst, Pingdingshan coalfield, northern China. *Int. J. Coal Geol.* 47 (2), 101–113. doi:10.1016/S0166-5162(01)00031-3

Li, M. (2013). *Structure evolution and deformation mechanism of tectonically deformed coal*. Xuzhou: China University of Mining and Technology. (In Chinese with English Abstract).

Li, Y., Song, D., Liu, S., and Pan, J. (2020). Characterization of ultramicropores and analysis of their evolution in tectonically deformed coals by Low-Pressure CO2 adsorption, XRD, and HRTEM techniques. *Energy fuels.* 34 (8), 9436–9449. doi:10.1021/acs.energyfuels.0c01403

Liu, H., Hou, C., and Song, Y. (2022). Molecular dynamics simulation of the nanoindentation of coal vitrinite. *Front. Earth Sci.* 10. doi:10.3389/feart.2022.856290

Liu, H., Jiang, B., Liu, J., and Song, Y. (2018). The evolutionary characteristics and mechanisms of coal chemical structure in micro deformed domains under sub-high temperatures and high pressures. *Fuel* 222, 258–268. doi:10.1016/j.fuel.2018.02.117

Liu, H., Jiang, B., Song, Y., and Hou, C. (2019). The tectonic stress-driving alteration and evolution of chemical structure for low- to medium-rank coals-by molecular simulation method. *Arab. J. Geosci.* 12 (23), 1–16. doi:10.1007/s12517-019-4909-8

Liu, H., and Jiang, B. (2019). Stress response of noncovalent bonds in molecular networks of tectonically deformed coals. *Fuel* 255, 115785. doi:10.1016/j.fuel.2019.115785

Liu, H. (2020). *The dynamic differentiation characteristics and mechanisms of stress-sensitive elements and minerals in tectonically deformed coals*. Xuzhou: China University of Mining and Technology. (In Chinese with English Abstract).

Mattsson, T. R., Lane, J. M. D., Cochrane, K. R., Desjarlais, M. P., Thompson, A. P., Pierce, F., et al. (2010). First-principles and classical molecular dynamics simulation of shocked polymers. *Phys. Rev. B* 81 (5). doi:10.1103/PhysRevB.81.054103

Meng, J., Cao, Z., Zhang, S., Wang, C., and Nie, B. (2021). Micro-mechanical properties and damage mechanisms of coal under cyclic loading: A nanoindentation experiment and molecular dynamics simulation. *Mol. Simul.* 48, 354–365. doi:10.1080/08927022.2021.2015070

Niu, Q., Pan, J., Cao, L., Ji, Z., Wang, H., Wang, K., et al. (2017). The evolution and formation mechanisms of closed pores in coal. *Fuel* 200, 555–563. doi:10.1016/j.fuel.2017.03.084

Pan, J., Mou, P., Ju, Y., Wang, K., Zhu, Q., Ge, T., et al. (2022). Micro-nano-scale pore stimulation of coalbed methane reservoirs caused by hydraulic fracturing experiments. *J. Petroleum Sci. Eng.* 214, 110512. doi:10.1016/j.petrol.2022.110512

Plimpton, S. (1995). Fast parallel algorithms for short-range molecular dynamics. *J. Comput. Phys.* 117, 1–19. doi:10.1006/jcph.1995.1039

Qiang, Y., Wu, W., Lu, J., Jiang, B., and Ziegmann, G. (2020). Progressive molecular rearrangement and heat generation of amorphous polyethene under sliding friction: Insight from the United-Atom molecular dynamics simulations. *Langmuir* 36 (38), 11303–11315. doi:10.1021/acs.langmuir.0c01949

Rittel, D. (2000). An investigation of the heat generated during cyclic loading of two glassy polymers. Part I: Experimental. *Mech. Mater.* 32 (3), 131–147. doi:10.1016/S0167-6636(99)00051-4

Song, Y., Jiang, B., Li, M., Hou, C., and Mathews, J. P. (2020). Macromolecular transformations for tectonically-deformed high volatile bituminous via HRTEM and XRD analyses. *Fuel* 263, 116756. doi:10.1016/j.fuel.2019.116756

Song, Y., Jiang, B., and Qu, M. (2019). Macromolecular evolution and structural defects in tectonically deformed coals. *Fuel* 236, 1432–1445. doi:10.1016/j.fuel.2018.09.080

van Duin, A. C. T., Dasgupta, S., Lorant, F., and Goddard, W. A. (2001). ReaxFF: A reactive force field for hydrocarbons. *J. Phys. Chem. A* 105 (41), 9396–9409. doi:10.1021/jp004368u

Wang, J., Han, Y., Chen, B., Guo, G., Hou, Q., and Zhang, Z. (2017). Mechanisms of methane generation from anthracite at low temperatures: Insights from quantum chemistry calculations. *Int. J. Hydrogen Energy* 42 (30), 18922–18929. doi:10.1016/j.ijhydene.2017.06.090

Wang, J., Hou, Q., Zeng, F., and Guo, G. (2021). Gas generation mechanisms of bituminous coal under shear stress based on ReaxFF molecular dynamics simulation. *Fuel* 298, 120240. doi:10.1016/j.fuel.2021.120240

Wang, J., Hou, Q., Zeng, F., and Guo, G. (2021). Stress sensitivity for the occurrence of coalbed gas outbursts: A reactive force field molecular dynamics study. *Energy fuels.* 35, 5801–5807. doi:10.1021/acs.energyfuels.0c04201

Xu, R., Li, H., Guo, C., and Hou, Q. (2014). The mechanisms of gas generation during coal deformation: Preliminary observations. *Fuel* 117, 326–330. doi:10.1016/j.fuel.2013.09.035

Yang, Y., Pan, J., Hou, Q., Wang, K., and Wang, X. (2021). Stress degradation mechanism of coal macromolecular structure: Insights from molecular dynamics simulation and quantum chemistry calculations. *Fuel* 303, 121258. doi:10.1016/j.fuel.2021.121258

Yang, Y., Pan, J., Wang, K., and Hou, Q. (2020). Macromolecular structural response of Wender coal under tensile stress via molecular dynamics. *Fuel* 265, 116938. doi:10.1016/j.fuel.2019.116938

Yu, S., Bo, J., Vandeginste, V., and Mathews, J. P. (2022). Deformation-related coalification: Significance for deformation within shallow crust. *Int. J. Coal Geol.* 256, 103999. doi:10.1016/j.coal.2022.103999

Zhang, J., Chu, X., Wei, C., Zhang, P., Zou, M., Wang, B., et al. (2022). Review on the application of Low-Field nuclear magnetic resonance technology in coalbed methane production simulation. *ACS Omega* 7, 26298–26307. doi:10.1021/acsomega.2c02112

Zhang, J., Wei, C., Ju, W., Yan, G., Lu, G., Hou, X., et al. (2019). Stress sensitivity characterization and heterogeneous variation of the pore-fracture system in middle-high rank coals reservoir based on NMR experiments. *Fuel* 238, 331–344. doi:10.1016/j.fuel.2018.10.127

Zhang, J., Wei, C., Zhao, C., Zhang, T., Lu, G., and Zou, M. (2021). Effects of nano-pore and macromolecule structure of coal samples on energy parameters variation during methane adsorption under different temperature and pressure. *Fuel* 289, 119804. doi:10.1016/j.fuel.2020.119804